Proceedings of 5th Joint US-European Fluids Engineering Division Summer Meeting
FEDSM 2018
July 15-20, 2018, Montreal, Canada

FEDSM2018-83477

CALCULATION OF FRICTION FACTORS AND NUSSELT NUMBERS FOR TWISTED ELLIPTICAL TUBE HEAT EXCHANGERS USING NEK5000

Dillon R. Shaver
Argonne National Laboratory
Argonne, Illinois, USA
Email: dshaver@anl.gov

Lane B. Carasik
Kairos Power LLC
Oakland, California, USA
Email: carasik@kairospower.com

Elia Merzari
Argonne National Laboratory
Argonne, Illinois, USA
Email: emerzari@anl.gov

Nate Salpeter
Kairos Power LLC
Oakland, California, USA

Edward Blandford
Kairos Power LLC
Oakland, California, USA

ABSTRACT

The development of fluoride salt-cooled high-temperature reactors (FHRs) for nuclear power generation relies on the development of new technologies. Of the potential options being explored, twisted elliptical tube geometries for heat exchanger design are promising based on usage in other industries. They are expected to offer significant enhancement in heat transfer with only a marginal increase in frictional losses. This allows them to be deployed in relatively compact designs that are well suited for FHRs. The presented work focuses on the computational fluid dynamics (CFD) simulations of heated molten salt flows through various twisted elliptical tube geometries at low modified Froude numbers. The objectives of this work are to evaluate the available correlations at lower Froude numbers and to determine the impact of using non-zero tube to tube spacing to resolve contact points or numerical singularities for future CFD simulations efforts. The spectral element CFD code Nek5000 was used for all simulations, which were performed in periodic domains of triangular (hexagonal) and square unit cells surrounding a single tube through a complete twist using an explicit filtering large eddy simulation (LES) method. Simulations were used to parametrically test the effects of tube-to-tube spacing for laminar and turbulent flow regimes on frictional pressure drop and heat transfer. The tested Reynolds numbers covered both laminar flow and fully developed turbulent flow ($90 < Re < 12200$*). The tested* S_L/d_{max} *ratios cover the range of 1.02 to 1.08 for both unit cell types.*

At moderate Reynolds number and comparitively high modified Froude number, excellent agreement for the Nusselt number was observed between simulations and the applicable correlation. As Froude number was decreased towards the bounds of the correlation, the agreement worsened. Cases were then simulated at low Froude number, testing the effects of tube spacing. It was determined that the laminar case for the square unit cell is the most affected by increasing S_L/d_{max} *and the gap size should be minimized to mitigate this. Whereas in the triangular unit cell the laminar flow regime is more significantly impacted by increasing* S_L/d_{max} *compared to the turbulent flow regime which was only marginally impacted.*

NOMENCLATURE

A_{xs}	Cross sectional area
c_p	Specific heat
d	Tube diameter
D_h	Hydraulic diameter
f	Darcy friction factor
Fr_m	Modified Froude number

L	Length of a single twist (torsional pitch)
Nu	Nusselt number
P	Pressure
Pe	Peclet number
Pr	Prandtl number
q''_w	Wall heat flux
Re	Reynolds number
S_T	Tube center-to-center distance
T	Temperature defect
$\hat{T}$	Temperature
t	Time
$\vec{u}$	Local velocity (vector)
U	Mean velocity
γ	Temperature periodicity parameter
λ	Thermal conductivity
μ	Molecular viscosity
ν	Kinematic viscosity
Π_w	Wetted perimeter
ρ	Density

Subscripts

f	Final
0	Initial
max	Maximum
min	Minimum
sq	Square array
tri	Triangular array
w	Wall quantity

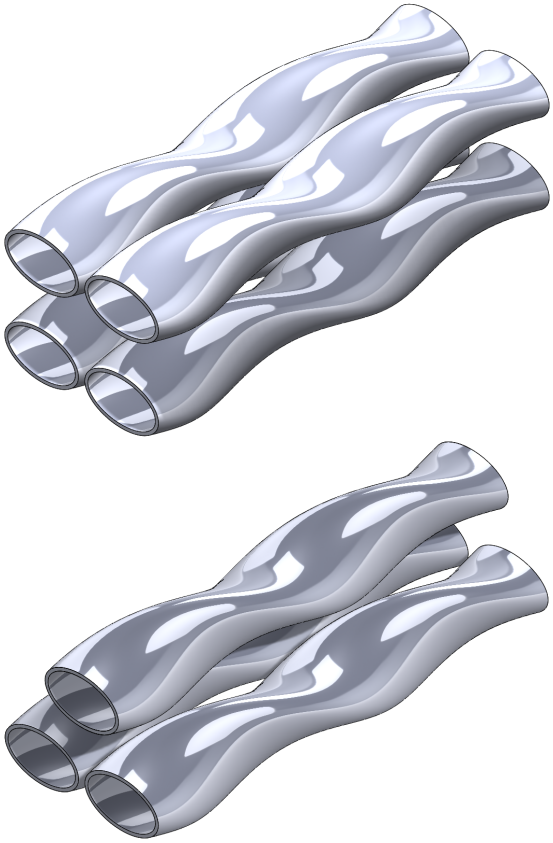

FIGURE 1. TWISTED-ELLIPTICAL-TUBE BUNDLES SHOWING (TOP) A SQUARE ARRAY AND (BOTTOM) A TRIANGULAR ARRAY

INTRODUCTION

To enable deployment of the flouride salt-cooled high-temperature reactor concept, researchers are investigating new technologies from all fields of engineering. One of the innovative heat exchanger technologies being explored is the twisted-elliptical-tube heat exchanger, which has been used by the oil and natural gas industries. These industries see the usage of high Prandtl number working fluids, which is typical of working fluids for FHRs. The twisted-elliptical-tube heat exchangers are found to have improved heat transfer and a marginal pressure drop increase from inherent turbulence inducing geometric features [1]. A schematic of a twisted-elliptical-tube bundle for both triangular and square unit cells is shown in Fig. 1.

Previous investigations on twisted-elliptical-tube heat exchangers have been primarily experimental by Dzyubenko, Tan, Yang and others [2–7]. A comprehensive review of these works was done by Hughes [8]. These works have demonstrated a fairly strong dependence of frictional pressure drop and heat transfer on the torsional length, or more specifically, the modified Froude number. However, for lower Froude numbers ($\sim$64) on the shell side, these correlations do not readily apply and are a focus of this work which is discussed later.

The current available literature for numerical investigations on twisted-elliptical-tubes is found to be quite scarce. Previous numerical efforts for both tube [4, 6] and shell side flows [9] were conducted using RANS with either the standard κ-ε, Realizable κ-ε, or κ-ω Shear Stress Transport turbulence models. The shell side flow which is the focus of this current work was previously investigated with the Standard and Realizable κ-ε turbulence models by Tan et al. [9]. Tan et al. investigated the impact on heat transfer and pressure drop from varying the ratio of outer major/minor diameters and torsional pitch for a hexagonal/triangular array of tubes.

The twisted-elliptical-tubes are arranged such that the tubes are touching in the twisted regions to provide structural support. This touching in the form of contact points are difficult to simulate due to being a numerical singularity that cannot be handled directly. The contact points between the tubes must be modeled in some form using a few different techniques. Typically, this modeling is done by leaving a small finite gap at the con-

tact points or by increasing the contact point to have a small finite area. Previous numerical works on the shell side of twisted-elliptical-tubes did not investigate the impact of treatment for the contact point between the tubes. This has been investigated numerically in wire-wrapped nuclear fuel rod geometries that indicate that at low Prandtl numbers (~ 0.01), the effects of the point contact are minimal [10]. However, molten salts have significantly higher Prandtl numbers (~ 10) and may exhibit different behavior.

An overarching goal of this study is to examine the applicability of the known correlations to lower Froude number geometries in order to evaluate their potential use in heat exchanger design under these conditions through simulation. To enable this goal, the impact or effect of the point contact modeling is investigated through the usage of a small finite gap and varied between simulations. This is achieved by varying the center-to-center distance (pitch) of the twisted-elliptical-tubes and is presented as the ratio between pitch and the maximum diameter of the twisted-elliptical-tube. The effects are quantified by calculating the Darcy friction factor and the bulk Nusselt number. This is done for various values of this ratio at both a low Reynolds number (laminar) and a high Reynolds number (fully turbulent).

Geometric Parameters and Nondimensional Numbers

The twisted-elliptical-tube geometry discussed in this work is a tube formed with an elliptical cross-section. Some of the key geometric parameters are shown on a triangular unit cell of elliptical cross-sections in Fig. 2.

The Reynolds number for these flows is defined from the mean velocity, viscosity, and hydraulic diameter as

$$Re = \frac{UD_h}{\nu}. \tag{1}$$

The hydraulic diameter is calculated from the standard expression

$$D_h = \frac{4A_{xs}}{\Pi_w}, \tag{2}$$

where A_{xs} is the cross-sectional area and Π_w is the wetted perimeter. The cross-sectional area for the square and triangular unit cells were calculated by using

$$A_{xs,sq} = S_T^2 - \frac{\pi}{4} d_{max} d_{min} \tag{3}$$

and

$$A_{xs,tri} = \frac{1}{2}\left[\frac{S_T^2}{2\tan\left(\frac{\pi}{6}\right)} - \frac{\pi}{4} d_{max} d_{min}\right], \tag{4}$$

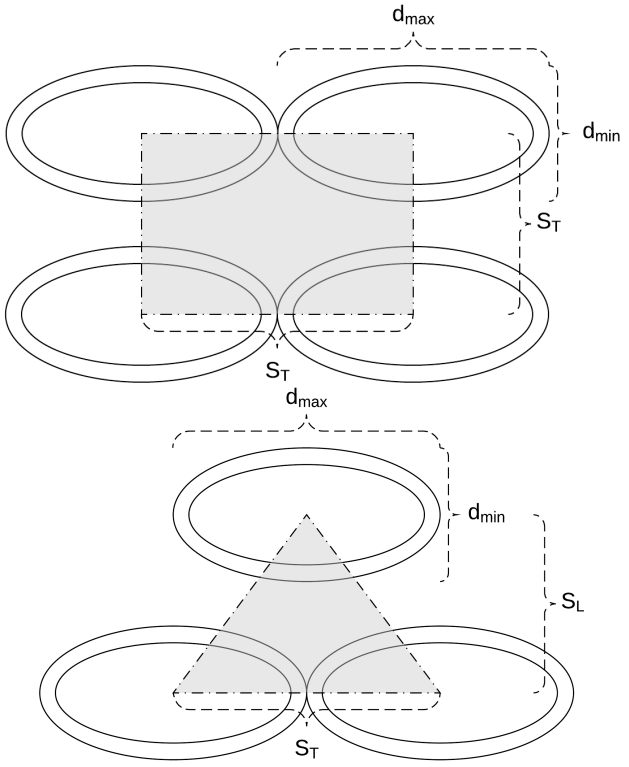

FIGURE 2. SQUARE AND TRIANGULAR UNIT CELLS OF TWISTED-ELLIPTICAL-TUBES

where S_T is center-to-center distance between two tubes (transverse pitch). The wetted perimeter for the square and triangular unit cells were calculated by using

$$\Pi_{w,sq} = \pi \left[3\left(\frac{d_{max}}{2} + \frac{d_{min}}{2}\right) - \sqrt{\left(\frac{3d_{max}}{2} + \frac{d_{min}}{2}\right)\left(\frac{d_{max}}{2} + \frac{3d_{min}}{2}\right)} \right] \tag{5}$$

and

$$\Pi_{w,tri} = \frac{\Pi_{w,sq}}{2}. \tag{6}$$

The torsional pitch for a twisted-elliptical-tube is defined as the length of a full 2π twist. It is used in calculating the modified Froude number (swirl number).

$$Fr_m = \frac{L^2}{d_{max} D_h} \tag{7}$$

Friction Factor Correlations

The available friction factor correlations applicable to external side of the twisted-elliptical-tubes were developed by Dzyubenko [3]. The Darcy friction factor is calculated by using the following equation for transitional to turbulent regimes of flow

$$f = 0.3164 Re^{-0.25} \left(1 + 3.6 Fr_m^{-0.357}\right). \tag{8}$$

This correlation is considered valid for any flows and geometries for $Re \geq 800$ and $Fr_m \geq 100$.

For transitional flow regimes with low Froude numbers, the following correlation is recommended

$$f = 89.4 Re^{[-1.2322 + 0.121 \log_{10}(Re)]} \tag{9}$$

which is valid for $Fr_m = 63.6$, $Re \geq 100$.

Nusselt Number Correlations

The currently available heat transfer correlations for the shell side of twisted-elliptical-tubes cover laminar, transitional, and turbulent flow ranges for a variety of geometric properties. Each equation was modified from the original references to account for liquids as opposed to gases as recommended by Hughes [8]. This modification is done by replacing the wall-to-bulk temperature ratio with the corresponing viscosity ratio.

$$\left(\frac{\hat{T}_w}{\hat{T}_b}\right)^{-0.55} \rightarrow \left(\frac{\mu_w}{\mu_b}\right)^{-0.14} \tag{10}$$

In practice, this factor is quite small. It was treated as unity for the evaluation of all correlations, which corresponds with the constant properties assumption used in the simulations.

For the transitional regime of flow, the Dzyubenko transitional Nusselt number correlation [3] is as follows

$$Nu_{Dzy,trans} = 83.5 Fr_m^{-1.2} Re^n Pr^{0.4} \left(1 + 3.6 Fr_m^{-0.357}\right) \left(\frac{\mu_w}{\mu_b}\right)^{-0.14} \tag{11}$$

where

$$n = 0.212 Fr_m^{0.194}. \tag{12}$$

This correlation is considered valid for any flows and geometries for $Re < 3000$ and $63.6 \leq Fr_m < 924$.

For the turbulent regime of flow, the Dzyubenko [3], Ievlev [2], and Ievlev-2 [2] correlations are used. The Dzyubenko correlation is stated in the following equation:

$$Nu_{Dzy} = 6.05(10^6) Fr_m^{\alpha} Re^{\beta} Pr^{0.4} \left(\frac{\mu_w}{\mu_b}\right)^{-0.14}, \tag{13}$$

where

$$\alpha = -2.494 + 0.235 \log_{10}(Fr_m), \tag{14}$$

$$\beta = Re^{\varepsilon} + \eta \log_{10}(Re), \tag{15}$$

$$\varepsilon = -1.572 Fr_m^{[0.01661 - 0.04373 \log_{10}(Fr_m)]}, \tag{16}$$

and

$$\eta = 0.269 Fr_m^{[-0.01490 - 0.0104 \log_{10}(Fr_m)]}. \tag{17}$$

This correlation is considered valid for any flows and geometries with $2000 \leq Re \leq 30{,}000$ and $63.6 \leq Fr_m \leq 1150$. The first Ievlev correlation is stated as follows.

$$Nu_{Ivl,1} = 0.023 Re^{0.8} Pr^{0.4} \left(1 + 3.6 Fr_m^{-0.357}\right) \left(\frac{\mu_w}{\mu_b}\right)^{-0.14} \tag{18}$$

This correlation is considered valid for any flows and geometries with $2000 \leq Re \leq 50{,}000$ and $232 \leq Fr_m \leq 2440$. The second Ievlev correlation is stated as follows.

$$Nu_{Ivl,2} = 0.0521 Re^{0.8} Pr^{0.4} \left(\frac{\mu_w}{\mu_b}\right)^{-0.14} \tag{19}$$

which is considered valid for any flows and geometries with $2000 \leq Re \leq 50{,}000$ and $Fr_m = 64$. The Nusselt number correlations and their applicable ranges are summarized in Tab. 1.

NUMERICAL METHOD

Details of the modeling and simulation method are described below.

TABLE 1. APPLICABILITY RANGES FOR THE PRESENTED NUSSELT NUMBER CORRELATIONS

Correlation	Re range	Fr_m range
Eqn. (11)	$Re < 3000$	$63.6 \leq Fr_m < 924$
Eqn. (13)	$2000 \leq Re \leq 3(10^4)$	$63.6 \leq Fr_m < 1150$
Eqn. (18)	$2000 \leq Re \leq 5(10^4)$	$232 \leq Fr_m < 2440$
Eqn. (19)	$2000 \leq Re \leq 5(10^4)$	$Fr_m \sim 64$

The Nek5000 CFD Code

Nek5000 [11] is an open source CFD code based on the spectral element method [12]. It is written in both FORTRAN 77 and C with parallelization implemented via MPI and a third party gather-scatter library [13]. The spectral element method (a subset of the finite element method) is implemented for spatial discretization and explicit time-marching schemes can be used to solve the unsteady Navier-Stokes equations. Nek5000 has the capabilities to perform direct numerical simulations (DNS), large eddy simulations (LES), and unsteady Reynolds-averaged Navier-Stokes (uRANS) simulations. The code has been extensively used and validated for high fidelity simulations of heat transfer in complex geometries [14, 15] This work focuses on the LES methodology because of its balance between accuracy and reasonable computational and time requirements. Nek5000 can solve the low-Mach form of the unsteady Navier-Stokes with variable fluid properties. For this work, however, all fluid properties were assumed constant.

Governing Equations and Associated Formulation

The specific formulation of the Navier-Stokes and energy equations used for these simulations are shown below. The momentum equation is given by

$$\rho\left(\frac{\partial \vec{u}}{\partial t}+\vec{u}\cdot\nabla\vec{u}\right)=-\nabla P+\mu\nabla^2\vec{u}, \tag{20}$$

where the divergence constraint on velocity is

$$\nabla\cdot\vec{u}=0. \tag{21}$$

The form of the energy equation is given by

$$\rho c_p\left(\frac{\partial \hat{T}}{\partial t}+\vec{u}\cdot\nabla\hat{T}\right)=\lambda\nabla^2\hat{T}. \tag{22}$$

All simulations were nondimensionalized such that D_h, U, ρ, and c_p were all equal to 1. This implies that $\mu = 1/Re$, and $\lambda = 1/Pe$, where the Peclet number is $Pe = RePr$.

TABLE 2. GEOMETRIC PARAMETERS OF THE SIMULATIONS

Parameter	Value
$\frac{d_{min}}{d_{max}}$	0.62
$\frac{L}{d_{max}}$	8.086
$\frac{S_T}{d_{max}}$	1.02 – 1.08
$Fr_{m,sq}$	62.1 – 76.19
$Fr_{m,tri}$	80.6 – 101.8

The spatial discretization is a two-step process involving the initial domain discretization into elements. Gauss-Legendre-Lobatto (GLL) quadrature points are then mapped inside each element, which are defined by the polynomial approximation order ($\mathbb{P}_N$) for each simulation. The total number of degrees of freedom for each simulation can be roughly calculated as $\mathbb{P}_N^3$. The temporal discretization is done through a third-order BDF/EXT time stepping explicit scheme.

The velocity and temperature equations are solved in their dimensionless forms by using the default Helmholtz solver with a numerical residual tolerance of 10^{-7}, and a Poisson equation is solved for the pressure field with a tolerance of 10^{-5}. The implemented LES model uses an explicit low-pass filter, effectively removing energy from the smallest simulated scales [16].

Geometry Details

The twisted elliptical tube geometry used in these simulations are characterized by geometric ratios involving the tube minimum and maximum diameters of a cross section, torsional pitch, and tube pitch. These are summarized in Tab. 2.

Mesh Creation and Computational Domain

A base mesh was generated for both the square and triangular unit cells using prenek, one of the native meshing tools included with the Nek5000 distribution. The base mesh consisted of an extruded cylindrical tube surrounded by either a hexagonal or square domain. The cylindrical tube and surrounding mesh were distorted into the twisted-tube shape at runtime. Front views of the final meshes for both array types are shown in Fig. 3, which encompasses the fluid domain in the space between the tubes shown in Fig. 1.

A mesh convergence study was performed independently for each array type by varying the polynomial approximation order, also known as a p-type mesh study. These have been demonstrated to be identical to h-type, or element-based, refinement

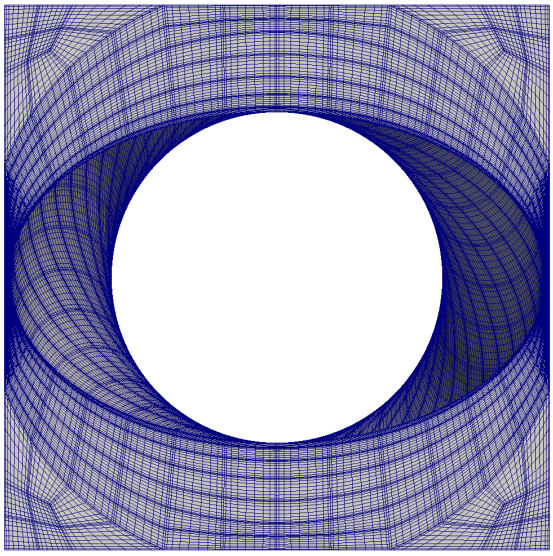

(a) SQUARE ARRAY

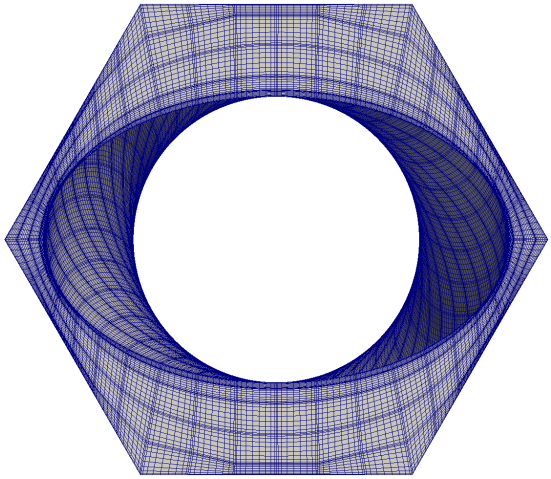

(b) TRIANGULAR ARRAY

FIGURE 3. FRONT VIEW OF THE 9th ORDER MESHES USED FOR (a) THE SQUARE ARRAY AND (b) THE TRIANGULAR ARRAY, BOTH SHOW THE DISTRIBUTION OF THE GAUSS-LOBATTO-LEGENDRE QUADRATURE POINTS

studies, however the p-type has the advantage of converging exponentially, rather than algebraically. This was done at the respective high Reynolds number conditions with all pitch-to-diameter ratios. For both the square and triangular arrays the polynomial approximation was tested at 7^{th}, 9^{th}, and 11^{th} orders. The study was performed by starting the simulation at a lower order until the initial transient was washed out, then progressively increasing the polynomial order. The results showed little variation with less than 5% variation between 7^{th} and 9^{th} orders and less than 2% between 9^{th} and 11^{th}. The 9^{th} order discretization was determined to be sufficient.

Boundary Conditions

The boundary conditions were set to periodic for all boundaries except for the no-slip wall which included a constant heat flux of $q''_w/(U\rho c_p) = 1$. The mean flow direction was oriented along the z-axis. A constant mean velocity was maintained by imposing a source in the z-momentum equation, which is interpreted as an imposed pressure gradient. This momentum source is calculated automatically by Nek5000 for each time step by solving the corresponding Stokes problem with a unity pressure gradient and scaling the result as necessary. No further special treatment of the pressure equation is necessary.

The boundary condition for the energy equation in the z-direction is non trivial [15] and is given by

$$\hat{T}(x,y,0,t) + \gamma L = \hat{T}(x,y,L,t). \tag{23}$$

The global energy balance can be used to construct an expression for γ, which yields

$$\gamma = \frac{q''_w}{\rho c_p}\frac{A_w}{VU}, \tag{24}$$

where V is the volume of the fluid domain and A_w is the wall area. A new variable is then substituted for the temperature which does satisfy the periodic boundary condition

$$\hat{T} = T + \gamma z. \tag{25}$$

This is combined with the energy equation to yield a governing equation for the temperature defect

$$\rho c_p\left(\frac{\partial T}{\partial t} + \vec{u}\cdot\nabla T\right) = \lambda\nabla^2 T - \rho c_p \gamma u_z, \tag{26}$$

which has true periodic boundary conditions in all directions.

Data Processing and Reduction

In order to obtain the time-averaged friction factors, the instantaneous values were calculated. An expression for the instantaneous friction factor was obtained from the Darcy-Weisbach equation

$$\frac{\Delta P}{L} = f\frac{\rho U^2}{2D_h}. \tag{27}$$

The required imposed pressure gradient to maintain flow at velocity U is substituted into the LHS to yield

$$f = 2\frac{\mathrm{d}P}{\mathrm{d}z}\frac{D_h}{\rho U^2}. \tag{28}$$

To obtain the average friction factor, these values are time averaged

$$\overline{f} = \frac{1}{t_f - t_0} \int_{t_0}^{t_f} f(t) \mathrm{d}t. \tag{29}$$

To obtain the average Nusselt numbers, the time-average temperature fields were first calculated. The average Nusselt number is then calculated from

$$\overline{Nu} = \frac{q''_w}{\overline{T_w} - \overline{T_b}} \frac{D_h}{\lambda} \tag{30}$$

where $\overline{T_w}$ and $\overline{T_b}$ are obtained in a similar manner as $\overline{f}$. The required time interval $(t_f - t_0)$ was tested for each case to ensure a fully converged result.

The procedure of calculating the instantaneous friction factor and Nusselt number was verified by testing it for laminar flow in a channel. The calculated values were consistent with theoretical values to within the solver tolerance.

RESULTS

Initially, a set of cases with a Reynolds number in the transitional range was simulated. This was done both to validate the method as well as examine the behavior of the correlations as the lower bound on Froude number is approached. For these initial cases, a Prandtl number of 1 was used to maintain consistency with the experimental conditions of the correlations.

Cases were then simulated at both a high and a low Reynolds number for each array type testing pitch-to-diameter ratios of 1.02, 1.04, 1.06, and 1.08 with a fluid Prandtl number of 9.48. Friction factors and Nusselt numbers were calculated for each case using the procedure described above. Results are presented for both laminar and fully turbulent cases.

Identification of Correlation Discrepancies

In order to validate the methodology, a case well within the bounds of the Dzyubenko correlation for transistional flows, Eqn. (11), was tested. This case has a Reynolds number of 1500, a Prandtl number of 1 and a modified Froude number of 476.5. Results for this case agree very well with the correlation. However, it was hypothesized that with decreasing Froude number, the accuracy of the correlation would quickly diminish [8]. This was tested by simulating three additional cases at $Re = 1500$ and $Pr = 1$. All four of these cases have the same S_L/d_{max} ratio of 1.02 and d_{min}/d_{max} ratio of 0.5. The Froude number was controlled by modifying the torsional pitch, L. The simulated Froude numbers, predicted Nusselt numbers from both Nek5000 as well as the Dzyubenko correlation for transitional flow, and the percent differences are given in Tab. 3. The same data is presented graphically in Fig. 4.

TABLE 3. PREDICTED AND CORRELATED NUSSELT NUMBERS FOR THE TRANSITIONAL CASES

Fr_m	Nek5000	Eqn. (11)	Percent difference
476.5	12.30	12.05	2.1%
268.0	13.93	14.89	6.7%
83.95	19.53	27.79	34.9%
11.45	33.72	135.2	120.2%

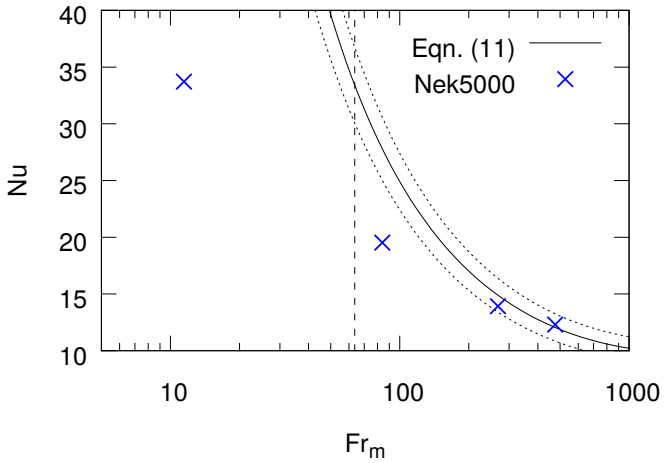

FIGURE 4. PREDICTED NUSSELT NUMBERS AT VARIOUS MODIFIED FROUDE NUMBERS COMPARED TO THE TRANSITIONAL FLOW CORRELATION OF DZYUBENKO, ····· INDICATES ±10%, - - - INDICATES LOWER RANGE OF EQN. (11).

It can be seen that the agreement between the correlation and Nek5000 is excellent for the case with the highest modified Froude number. This provides reasonable evidence that the formulation and method used with Nek5000 is consistent. As the Froude number is decreased, the agreement between the simulations and the correlation becomes worse. At $Fr_m = 268.0$, the agreement is still good, at a percent difference of under 7%. This case is still well above the reported minimum applicable Froude number. As the Froude number is further decreased to around 84, the percent difference becomes quite significant, with the simulations under-predicting the Nusselt by nearly 35% compared to the correlation. This is interesting as the correlation is reported to be valid to a Froude number as low as 63.6. It may suggest a different functional dependency on Froude number for these conditions. Finally, for a modified Froude number of 11.45, the correlation for transitional flow over predicts the Nusselt number by over 120%. However it is expected that the correlation would not be applicable to this case.

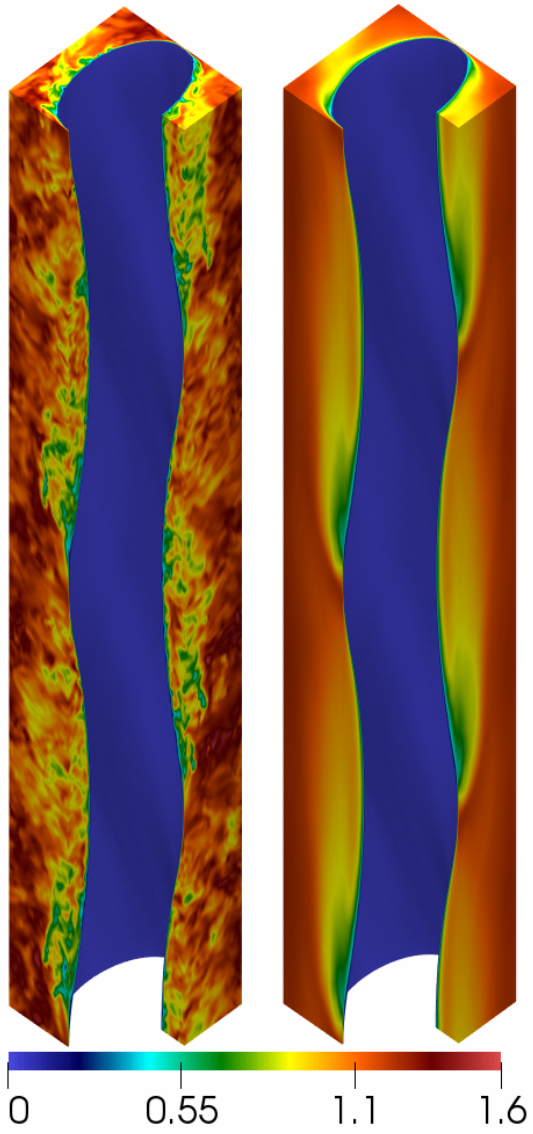

FIGURE 5. CFD RESULTS FOR $Re = 12200$ AND $S_L/d_{max} = 1.02$ IN THE SQUARE ARRAY SHOWING THE (LEFT) INSTANTANEOUS AND (RIGHT) AVERAGED VELOCITY FIELDS WITH A QUARTER OF THE DOMAIN REMOVED

Square Lattice

Simulations for the square lattice were carried out at Reynolds numbers of 120 and 12200 respectively for the laminar and turbulent conditions. Both the instantaneous and the averaged velocity fields for the turbulent case with $S_L/d_{max} = 1.02$ are shown in Fig. 5. Results for the friction factors and Nusselt numbers for the square array are tabulated in Tabs. 4 through 6, along with calculations from relevant correlations. Normalized results are plotted in Figs. 6 and 7 using the result for 1.02 pitch ratio as a reference.

TABLE 4. PREDICTED AND CORRELATED DARCY FRICTION FACTORS FOR THE SQUARE LATTICE

	$Re = 120$		$Re = 12200$	
S_L/d_{max}	Nek5000	Eqn. (9)	Nek5000	Eqn. (8)
1.02	0.7911	0.8174	0.0533	0.0532
1.04	0.8215	0.8174	0.0530	0.0538
1.06	0.8509	0.8174	0.0515	0.0544
1.08	0.8794	0.8174	0.0506	0.0549

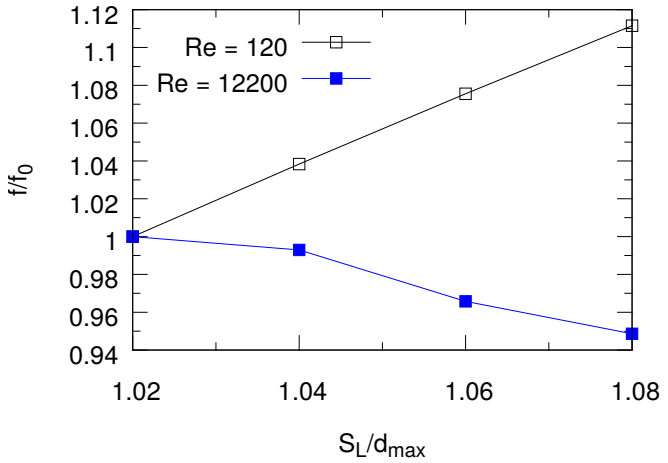

FIGURE 6. EFFECT OF S_L/d_{max} ON FRICTION FACTOR FOR THE SQUARE UNIT CELL

All of the predicted friction factors agree reasonably well with the applicable correlations, particularly the turbulent result at the highest S_L/d_{max}. It is worth noting that the correlation used for the laminar friction factors is applicable to a fixed Froude number, consequently Eqn. (9) has no dependency on Froude number, which changes slightly with S_L/d_{max}. As S_L/d_{max} increases, the associated hydraulic diameter increases, leading to a slightly smaller Froude number. The correlation for turbulent friction factor does include a dependency on Fr_m, however the simulations show worsening agreement with increasing S_L/d_{max}. It is likely that the correlations were developed for a fixed S_L/d_{max} of unity and the associated dependency on Fr_m and friction factor was not intended to be captured by these correlations.

From Tab. 4 and Fig. 6 the friction factor in laminar flow increases almost linearly with S_L/d_{max}. From 1.02 to 1.08, the friction factor increases by just over 11%. The opposite trend is observed in turbulent flow, with the friction factor decreasing by about 5% from across the range of pitch ratios. Interestingly, the decrease in turbulent friction factor is non-linear with the decreases between 1.02 to 1.04 and 1.06 to 1.08 being significantly

TABLE 5. PREDICTED AND CORRELATED NUSSELT NUMBERS FOR THE SQUARE LATTICE AT $Re = 120$

S_L/d_{max}	Nek5000	Eqn. (11)
1.02	8.288	21.03
1.04	9.036	22.44
1.06	9.619	23.88
1.08	10.09	25.35

TABLE 6. PREDICTED AND CORRELATED NUSSELT NUMBERS FOR THE SQUARE LATTICE AT $Re = 12200$

S_L/d_{max}	Nek5000	Eqn. (13)	Eqn. (19)
1.02	150.1	217.8	238.0
1.04	149.2	225.0	238.0
1.06	146.8	232.5	238.0
1.08	145.4	240.2	238.0

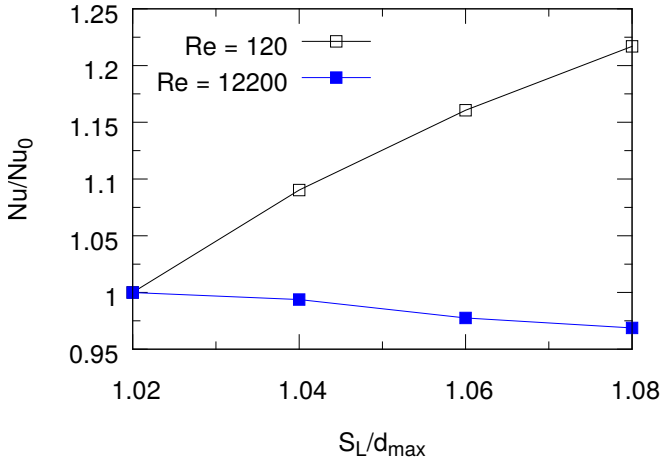

FIGURE 7. EFFECT OF S_L/d_{max} ON NUSSELT NUMBER FOR THE SQUARE UNIT CELL

less than the decrease from 1.04 to 1.06. Similar behavior is evident in the turbulent Nusselt numbers, shown in Fig. 7. This suggests the existance of some competing effects on the flow. The increased cross-secional area associated with the square lattice likely results in some suppression of the swirl effect as the flow has significant area available to bypass the region of influence of the tube.

From Fig. 7 and Tab. 5, the Nusselt number predictions for laminar cases in the square lattice show an increase as the pitch-to-diameter ratio increases. This is consistent with what is observed in the laminar friction factor but with a significantly greater increase of over 20%. The turbulent Nusselt number in contrast is practically unaffected by increasing S_L/d_{max}. The pitch-to-maximum-diameter ratio seems to have a much stronger effect on the laminar cases compared to the turbulent cases. This is somewhat expected, as the turbulent flow forms a much thinner boundary layer.

TABLE 7. PREDICTED AND CORRELATED DARCY FRICTION FACTORS FOR THE TRIANGULAR LATTICE

	$Re = 90$		$Re = 9000$	
S_L/d_{max}	Nek5000	Eqn. (9)	Nek5000	Eqn. (8)
1.02	1.079	1.013	0.0627	0.0549
1.04	1.130	1.013	0.0601	0.0556
1.06	1.179	1.013	0.0587	0.0563
1.08	1.224	1.013	0.0575	0.0569

Poor agreement between the Nusselt numbers predicted by simulations and correlations is observed for all cases. This was expected for the laminar results, as the available Dzyubenko correlation, Eqn. (11), is applicable for transitional flows. Although Dzyubenko notes that transition to a turbulent flow regime begins around $Re \approx 100$ [3], no signs of turbulence were observed in the simulations and these conditions would still fall at the extreme lower end of the transitional regime. It may be possible that effects of natural convection become significant under these conditions, which were not captured in the simulations.

Poor agreement was also somewhat expected for the turbulent results as the investigated Froude numbers also fall at the extreme lower end of the cited applicable conditions for the turbulent Dzyubenko correlation, Eqn. (13). This is consistent with the previously noted behavior observed at $Re = 1500$ when compared to the transitional Dzyubenko correlation. More surprising is the disagreement with the second Ievlev correlation, given by Eqn. (19). Despite only applying to a single Froude number, reasonable agreement should be expected as the Froude numbers for the simulations were quite close to the applicable value. Additionally, the Reynolds number is well within the reported range of applicability for the correlation.

Triangular Lattice

Simulations for the triangular lattice were carried out at Reynolds numbers of 90 and 9000 respectively for the laminar and turbulent conditions. Both the instantaneous and the averaged velocity fields for the turbulent case with $S_L/d_{max} = 1.02$ are shown in Fig. 8. Results for the friction factors and Nusselt numbers for the square array are tabulated in Tabs. 7 and 8, along with calculations from relevant correlations. Normalized results are plotted in Figs. 9 and 10 using the result for 1.02 pitch ratio as a reference.

All of the simulated friction factors agree somewhat well with the correlations. There is more discrepancy in the laminar friction factors compared to the square lattice, however the

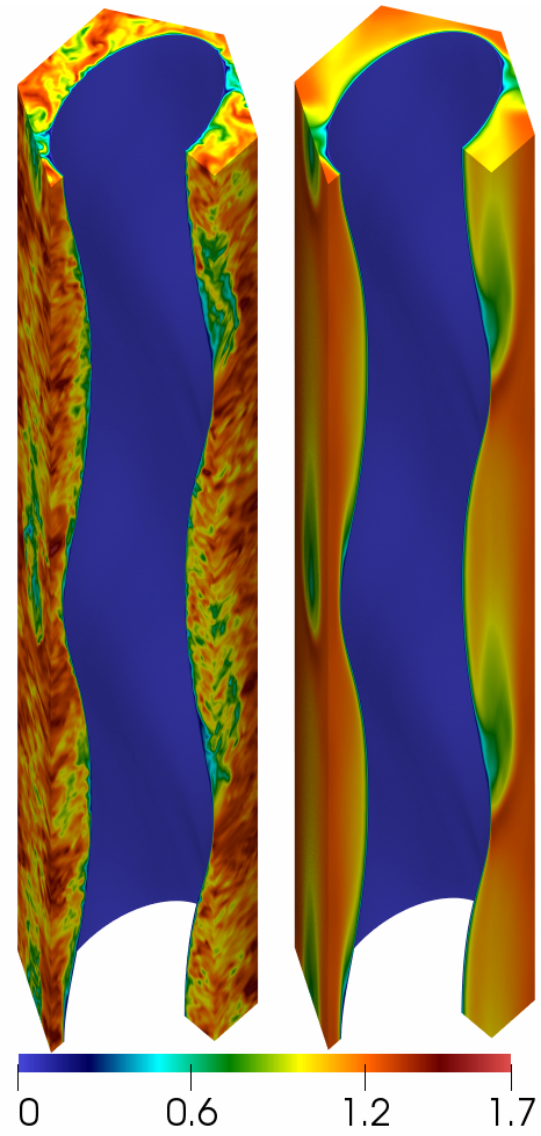

FIGURE 8. CFD RESULTS FOR $Re = 9000$ AND $S_L/d_{max} = 1.02$ IN THE TRIANGULAR ARRAY SHOWING THE (LEFT) INSTANTANEOUS AND (RIGHT) AVERAGED VELOCITY FIELDS WITH A QUARTER OF THE DOMAIN REMOVED

range of Froude numbers for the triangular lattice is much farther from the value of 63.6 required by the correlation as well, so this discrepency is understandable. There is also more discrepancy in the turbulent friction factors as compared to the square lattice. Interestingly, the higher S_L/d_{max} ratio agrees best with the correlation. This is opposite of what was observed with the square lattice. Although the same trend is observed with the simulated turbulent friction factors decreasing with increasing pitch-to-diameter ratio.

From Fig. 9 and Tab. 7, the laminar friction factor increases

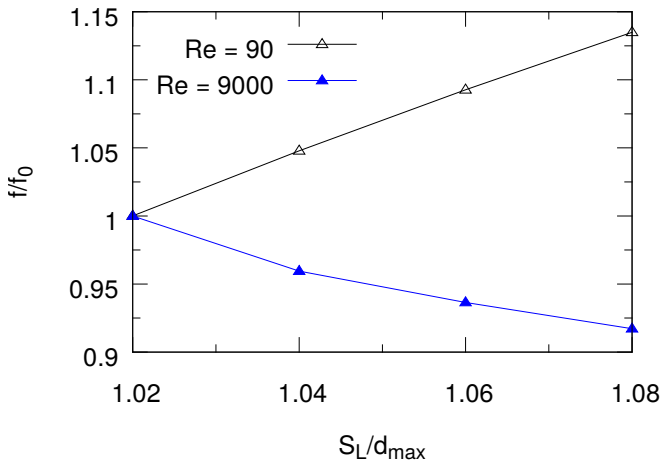

FIGURE 9. EFFECT OF S_L/d_{max} ON FRICTION FACTOR FOR THE TRIANGULAR UNIT CELL

TABLE 8. PREDICTED AND CORRELATED NUSSELT NUMBERS FOR THE TRIANGULAR LATTICE

	$Re = 90$		$Re = 9000$	
S_L/d_{max}	Nek5000	Eqn. (11)	Nek5000	Eqn. (13)
1.02	7.483	14.03	119.8	157.0
1.04	8.435	15.11	116.1	162.1
1.06	9.120	16.21	114.3	167.3
1.08	9.621	17.34	113.3	172.8

almost linearly with the pitch-to-diameter ratio, similarly to the square unit cell. From 1.02 to 1.08, the friction factor increases by approximately 13%. For the turbulent results, the friction factor decreases by about 8%, compared to only about 5% in the square lattice. The triangular unit cell does not show the same non-linear behavior with increasing pitch-to-diameter for the turbulent results that is seen for the square unit cell. This may be caused by the lack of a significant bypass area outside the region of influence of the twisted elliptical tubes.

Poor agreement was again observed between the Nusselt numbers predicted by simulations compared to the applicable correlation, particularly for the laminar results. As was the case for the square lattice, the available correlation for Nusselt number is intended for transitional flows and no evidence of turbulence was observed in the simulations at $Re = 90$. This Reynolds number is certainly lower than the reported onset of the transition to turbulent flow. It was therefore expected that the simulations and correlation would disagree.

For the turbulent results, the agreement between the Nusselt numbers predicted by simulations and the correlation is marginal at best. However, it is slightly better than the agreement for the square lattice with a range of percent differences of 27% to 42%.

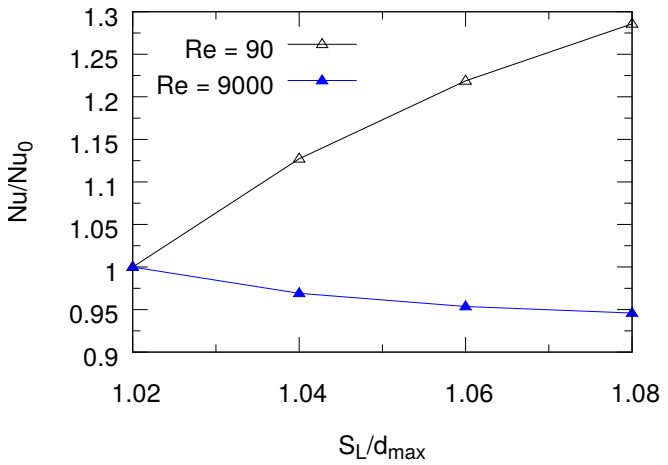

FIGURE 10. EFFECT OF S_L/d_{max} ON NUSSELT NUMBER FOR THE TRIANGULAR UNIT CELL

This is consistent with the observed behavior at lower Froude numbers as the triangular lattice has somewhat higher Froude numbers compared to the square lattice. If the trend shown in Fig. 4 holds, it would be expected for the percent differences between the simulated Nusselt numbers and the correlated values to be approximately 35%, and this is indeed what is observed.

From Fig. 10 and Tab. 8, the Nusselt number predictions for the laminar cases in the triangular unit cell are observed to increase as pitch-to-diameter ratio increases, following an almost identical trend as was seen in the square lattice. The laminar Nusselt number increases from 1.02 to 1.08 by just under 30% which is quite significant. The turbulent Nusselt number predictions are effectively insensitive to the pitch-to-diameter ratio, decreasing by just over 5%. As was observed in the square lattice, S_L/d_{max} has a much stronger influence on the laminar cases compared to the turbulent cases.

Nusselt numbers calculated from either Ievlev correlation, Eqns. (18 & 19) are not presented for these results as the modified Froude numbers are well outside the bounds for each. Although interestingly, the turbulent results for the triangular lattice showed the best agreement with the Ievlev correlation, Eqn. (18). The agreement was still fairly poor ($\sim$ 30% difference) and the fact that the Ievlev correlation apparently performed better than the others is likely only serendipitous.

CONCLUSIONS

A set of simulations of flow and heat transfer in twisted elliptical tube geometeries has been performed. The method was validated by simulating a case at a moderate Reynolds number and relatively high Froude number. This case was demonstrated to predict a Nusselt number in excellent agreement with the applicable correlation found in literature. It was further shown that at lower Froude numbers, this agreement becomes much worse. Additional cases were then simulated with low Froude numbers for both a square and a triangular unit cell to test the effect of pitch-to-maximum diameter ratio for the purposes of future CFD modeling.

Square Unit Cell

In the square unit cell, the friction factors were found to compare favorably with the correlations for both laminar and turbulent flow regimes. Increasing S_L/d_{max} for the laminar cases was observed to result in an overall increase of 11% for the friction factor, presenting a significant sensitivity. In the turbulent cases, increasing S_L/d_{max} caused an overall decrease of 5% in the friction factor, which is deemed insignificant.

The Nusselt numbers were found to be in poor agreement with the correlations for both laminar and turbulent flow regimes. However, this was somewhat expected. Increasing S_L/d_{max} for the laminar cases was observed to result in a signifcant increase in Nusselt number of over 20%. For the turbulent cases, increasing S_L/d_{max} resulted in a small overall decrease of less than 5%.

These findings suggest that changing the pitch-to-diameter ratio will have significant impacts in the laminar flow regime for the square unit cell and the pitch-to-maximum-diameter should not exceed 1.04 to mitigate this.

Triangular Unit Cell

For the triangular unit cell, the friction factors were again found to compare favorably with the correlations for both laminar and turbulent flow regimes. Increasing S_L/d_{max} for the laminar cases was observed to cause a significant overall increase of 13% in the friction factor. In the turbulent cases, increasing S_L/d_{max} caused an overall decrease of 8%.

As in the square unit cell, the Nusselt numbers were found to be in poor agreement the correlations for the laminar flow regime and the turbulent flow regime Nusselt numbers were found to be in marginally better agreement. The turbulent results were found to under-predict the correlation predictions by an amount consistent with the observations at moderate Reynolds number. Increasing S_L/d_{max} for the laminar cases resulted in a quite significant overall increase of about 30% in the Nusselt number. The effect was less significant for the turbulent cases, which had an overall decrease of less than 5%.

Unfortunately, the gap modeling for both the laminar and turbulent cases for the triangular unit cell are sensitive to gap size. The laminar cases are the most sensitive especially for the friction factor and the pitch-to-maximum-diameter ratio should be kept as close to unity as possible. The turbulent cases were less sensitive, but the impact on friction factor is significant enough to warrant taking care to model the contact as accurately as possible.

ACKNOWLEDGMENT

This work was supported the U.S. Department of Energy's Gateway for Accelerated Innovation in Nuclear (GAIN) program. The material was based upon work supported by the U.S. Department of Energy, Office of Science, under contract DE-AG02-06CH11357.

We gratefully acknowledge use of the computing resources provided on Bebop, a high-performance computing cluster operated by the Laboratory Computing Resource Center at Argonne National Laboratory.

REFERENCES

[1] Butterworth, D., Guy, A. R., and Welkey, J. J., 1996. "Design and applications of twisted-tube exchangers". In European research meeting on the future needs and developments in heat exchanger technology – advances in industrial heat transfer, R. J. Berryman, ed., IChemE, pp. 87–95.

[2] Dzyubenko, B. V., and Ievlev, V., 1980. "Heat transfer and hydraulic resistance in an intertubular space of a heat exchanger with flow twisting". *Energitka Transp*, pp. 117–125.

[3] Dzyubenko, B. V., 2006. "Estimation of the thermo-hydraulic efficiency of heat exchanging apparatuses with twisted tubes". *Heat Transfer Research,* ***37***(4).

[4] Tan, X.-H., Zhu, D.-S., Zhou, G.-y., and Zeng, L.-D., 2012. "Experimental and numerical study of convective heat transfer in twisted oval tubes". *International Journal of Heat and Mass Transfer,* ***55***, pp. 4701–4710.

[5] Tan, X.-H., Zhu, D.-S., Zhou, G.-y., and Zeng, L.-D., 2013. "Heat transfer and pressure drop performance of twisted oval heat exchanger". *Applied Thermal Engineering,* ***50***, pp. 374–383.

[6] Tang, X., Dai, X., and Zhu, D., 2015. "Experimental and numerical investigation of convective heat transfer and fluid flow in twisted spiral tube". *Intl. J. Heat and Mass Transfer,* ***90***.

[7] Sheng, Y., Zhang, L., and Hong, X., 2011. "Experimental study on convective heat transfer and flow resistance characteristics of water flow in twisted elliptical tubes". *Applied Thermal Engineering,* ***31***, pp. 2981–2991.

[8] Hughes, J. T., 2017. "Experimental and Computational Investigations of Heat Transfer Systems in Flouride Salt-cooled High-temperature Reactors". Ph.D. Thesis, The University of New Mexico, Albuquerque, NM, May.

[9] Tan, X.-H., Zhu, D.-S., Zhou, G.-y., and Zeng, L.-D., 2013. "3d numerical simulation on the shell side heat transfer and pressure drop performances of twisted oval tube heat exchanger". *International Journal of Heat and Mass Transfer,* ***65***, pp. 244–253.

[10] Merzari, E., Pointer, W. D., Smith, J. G., Tentner, A., and Fischer, P., 2012. "Numerical simulation of the flow in wire-wrapped pin bundles: Effect of pin-wire contact modeling". *Nucl. Eng. and Design,* ***253***, pp. 374–386.

[11] NEK5000 Version 17.0. December 17, 2017. Argonne National Laboratory, Argonne, Illinois. Available: https://nek5000.mcs.anl.gov.

[12] Fischer, P. F., Lottes, J., Pointer, W. D., and Siegel, A., 2008. "Petascale algorithms for reactor hydrodynamics". In J. Phys. Conf. Series.

[13] gslib Version 1.0.1. November 15, 2017. Available: https://github.com/gslib/gslib/releases.

[14] Greiner, M., Faulkner, R. J., Van, V. T., Tufo, H. M., and Fischer, P. F., 2000. "Simulations of three-dimensional flow and augmented heat transfer in a symmetrically grooved channel". *J. Heat Transfer,* ***122***, pp. 653–660.

[15] Goering, A., 2016. "Numerical investigation of wire coil heat transfer augmentation". MS Thesis, UIUC, Urbana, IL.

[16] Fischer, P. F., and Mullen, J. S., 2001. "Filter-based stabilization for spectral element methods". In *Comptes Rendus de l'Academie des Sciences Paris*, Vol. 332 of *Serie I. Analyse Numerique*. pp. 265–270.